THE AMERICAN SOCIETY OF MECHANICAL ENGINEERS
345 E. 47th St., New York, N.Y. 10017

94-GT-213

EXPERIMENTAL AND COMPUTATIONAL RESULTS FROM THE NASA LEWIS LOW-SPEED CENTRIFUGAL IMPELLER AT DESIGN AND PART FLOW CONDITIONS

Randall M. Chriss
NASA Lewis Research Center
Cleveland, Ohio

Michael D. Hathaway
Vehicle Propulsion Directorate
U.S. Army Research Laboratory
Cleveland, Ohio

Jerry R. Wood
NASA Lewis Research Center
Cleveland, Ohio

ABSTRACT

The NASA Lewis Low-Speed Centrifugal Compressor (LSCC) has been investigated with laser anemometry and computational analysis at two flow conditions: the design condition as well as a lower mass flow condition. Previously reported experimental and computational results at the design condition are in the literature (Hathaway et al. 1993). In that paper extensive analysis showed that inducer blade boundary layers are centrifuged outward and entrained into the tip clearance flow and hence contribute significantly to the throughflow wake. In this report results are presented for a lower mass flow condition along with further results from the design case.

The data set contained herein consists of three-dimensional laser velocimeter results upstream, inside and downstream of the impeller. In many locations data have been obtained in the blade and endwall boundary layers. The data are presented in the form of throughflow velocity contours as well as secondary flow vectors.

The results reported herein illustrate the effects of flow rate on the development of the throughflow momentum wake as well as on the secondary flow. The computational results presented confirm the ability of modern computational tools to accurately model the complex flow in a subsonic centrifugal compressor. However, the blade tip shape and tip clearance must be known in order to properly simulate the flow physics. In addition, the ability to predict changes in the throughflow wake, which is largely fed by the tip clearance flow, as the impeller is throttled should give designers much better confidence in using computational tools to improve impeller performance.

NOMENCLATURE

$\hat{e}$	Unit vector
$\hat{g}$	Streamwise grid unit vector
$\hat{g}_M$	Meridional grid unit vector $(= (g_r\hat{e}_r + g_z\hat{e}_z)/\sqrt{g_r^2 + g_z^2})$
ΔH	Total enthalpy rise
J	Streamwise station index
$\dot{m}$	Mass flow rate
m/m_s	Non-dimensional shroud meridional distance (% chord)
N	Number of laser anemometer realizations
N_B	Number of blades
PS	Pressure surface
Δp	Blade static pressure differential
q	Relative dynamic pressure $(\frac{1}{2}\rho W^2)$
r	Radial position
r/r_e	Radius normalized by impeller exit tip radius
SS	Suction surface
U_t	Corrected impeller exit tip speed
V	Absolute velocity vector
V_M	Meridional velocity vector $(= V_r\hat{e}_r + V_z\hat{e}_z)$
W_{sec}	Relative secondary velocity vector $(= \hat{g} \times (W \times \hat{g}))$
V_T	Throughflow velocity $(= (V_M \cdot \hat{g}_M)\hat{g}_M)$
W	Relative velocity vector
z_c	Statistical confidence coefficient
ρ	Density
σ	Local standard deviation
ω	Impeller rotational speed

Superscripts

—	Ensemble average
′	Instantaneous value

Presented at the International Gas Turbine and Aeroengine Congress and Exposition
The Hague, Netherlands — June 13–16, 1994
This paper has been accepted for publication in the Transactions of the ASME
Discussion of it will be accepted at ASME Headquarters until September 30, 1994

Subscripts

r	Radial component
θ	Tangential component
z	Axial component

INTRODUCTION

The full potential of the centrifugal compressor is still not realized and its development lags that of its axial counterpart. Furthermore, the database containing flowfield measurements of centrifugal compressors is limited, and consists predominantly of two-dimensional measurements. Nevertheless, the measurements to date have greatly enhanced our understanding of the flow development in these machines. Some of the previous investigations involving flowfield measurements are discussed in the following.

Although detected and discussed earlier by Dean and Senoo (1960), Eckardt's laser measurements (1976) provided the first flowfield experimental evidence of the development of a "wake" of low momentum fluid near the suction surface/shroud corner of the blade passage. Krain (1988) and Krain and Hoffman (1989,1990) and Sipos (1991), in a hot-wire investigation, drew conclusions about the secondary flow by looking at cross passage views of relative flow angle contours. However, their assumption of constant throughflow velocity tends to fail in the wake where the secondary flows are strongest. Krain and Hoffman (1989) have studied the effect of shroud contour shape on throughflow wake size and demonstrated that the position of the wake in the channel is strongly dependent upon the diffusion of the main flow in the impeller. Krain (1981) found only a weak influence of a vaned diffuser on the impeller flow albeit with a large diffuser leading edge radius ratio (1.1). He found large flow fluctuation levels far downstream at the diffuser throat.

Fagan and Fleeter (1990), in a low speed mixed flow compressor, showed that wake location and momentum defect magnitude both changed with mass flow rate. Johnson and Moore (1983) studied a low speed, shrouded impeller and found that the wake behaved as predicted by secondary flow theory (Cumpsty, 1989). Farge and Johnson (1990) made a detailed study of backswept shrouded impellers in a low speed environment which indicated wake formation at the shroud suction surface corner as predicted by theory.

Adler and Levy (1979), in a study of low-speed backswept shrouded impellers, and Rohne and Banzhaf (1990), in a study of high-speed backswept impellers, concluded that the output flow with backsweep yielded a more uniform and stable flow compared with radial bladed impellers. Ahmed and Elder (1990) made measurements inside a small high speed backswept impeller with splitter blades at multiple speeds and flow rates. They found that the wake region moved toward the suction side as the flow rate was reduced and that their preliminary three-dimensional flow measurements indicated that three-dimensional effects were important.

In previously reported results from this compressor (Hathaway et al., 1993) extensive experimental and CFD analysis showed that the blade boundary layers in the inducer section are centrifuged outward and are entrained into the tip clearance flow which forms the throughflow momentum wake and that the wake is not a result of streamwise flow separation. The experimental and computational results presented herein were obtained at a lower mass flow condition for comparison with those previously reported results.

The data consist of three-dimensional laser velocimeter results upstream, inside and downstream of the impeller. The purpose of the investigation is to compare results at the two flow conditions in order to study details of the flow physics as well as to provide data for CFD studies. In many locations data have been obtained in the blade boundary layers and endwall tip clearance flow. The data are presented in the form of throughflow velocity contours as well as secondary flow vectors.

FACILITY AND INSTRUMENTATION

The Compressor

The test compressor is a backswept impeller (Fig. 1) with an exit corrected design tip speed of 153 m/s. The impeller has 20 full blades with a backsweep of 55° from the radial. The design mass flow rate is 30 kg/s (66 lbm/s) and the design corrected shaft speed is 1920 rpm. The inlet diameter is 870 mm and the inlet blade height is 218 mm. The exit diameter is 1524 mm and the exit blade height is 141 mm. The tip clearance between the impeller blade and the shroud is 2.54 mm and is constant from inlet to exit. This tip clearance is 1.8% of blade height at the impeller exit and 1.2% at the inlet. The blade surfaces are composed of straight-line elements from hub to tip. A vaneless diffuser was used for the laser anemometer investigation. This allows an axisymmetric boundary condition to be used in the numerical simulations. A complete description of the facility can be found in Wood et al. (1983), and Hathaway et al. (1992).

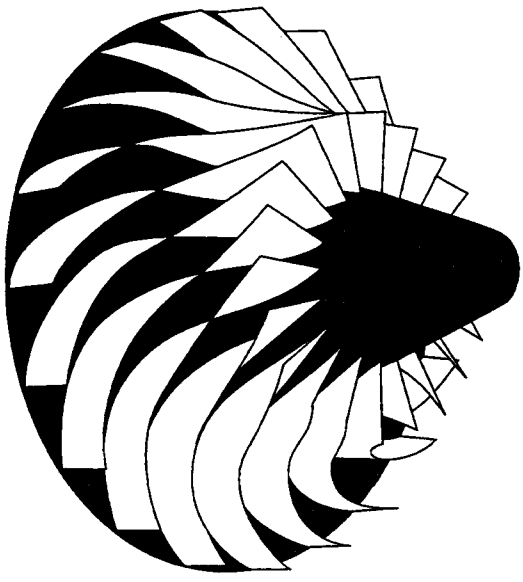

FIGURE 1. THE LARGE LOW SPEED IMPELLER.

The operating conditions for both the computational and experimental efforts are mass flow rates of 30.0 kg/s (66 lbm/s) and

23.6 kg/s (52 lbm/s) representing design and part flow conditions. For both conditions the corrected speed was fixed at 1862 RPM. The performance map is shown in Fig. 2. The differing symbols represent different downstream diffuser configurations as well as different spatial resolutions in the aerodynamic surveys. The uncertainty bars in the figure are based on mass flow and torque measurement limitations as well as a 0.6 K (1° R) thermocouple uncertainty.

In order to characterize the flow in the impeller with some relevant design parameters, a one-dimensional analysis of the impeller flow was undertaken. The results show that the diffusion ratio (given as the exit relative velocity divided by the inlet tip relative velocity) at the design flow, part flow and unstable condition was 0.75, 0.65 and 0.6 respectively. The absolute flow angle into the diffuser significantly influences the amount of pressure recovery that can be sustained by the diffuser. The diffuser entry flow angle from the radial for the three flow conditions was 67°, 74° and 77°, respectively.

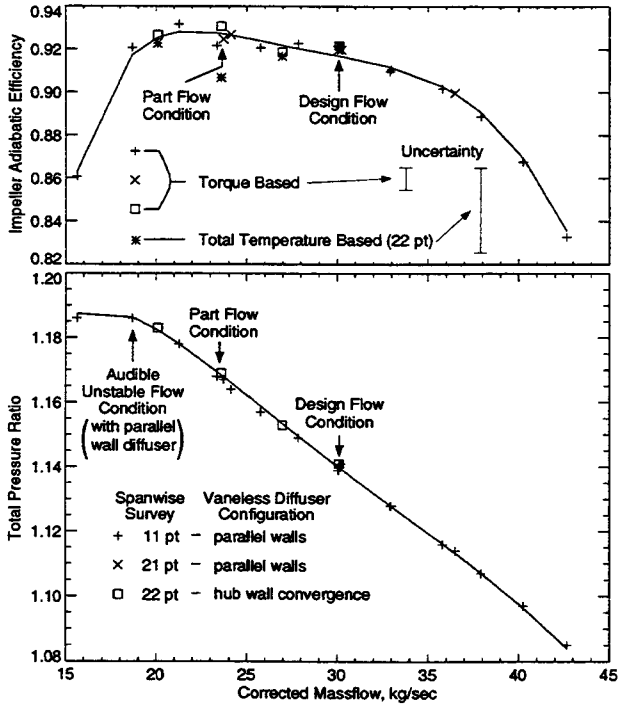

FIGURE 2. PERFORMANCE MAP FOR THE LARGE LOW SPEED CENTRIFUGAL IMPELLER.

Instrumentation

A two-component laser fringe anemometer operating in on-axis backscatter mode was used in this investigation. An Argon ion laser was used to produce the 514.5 nm (green) and 488 nm (blue) wavelengths for two orthogonal fringe systems. Frequency shifting was used for both fringe systems to provide directional sensitivity for all velocity measurements. Due to the size of the compressor a relatively long focal length of 733 mm was used. The final focusing lens aperture was 155 mm. In addition, beam expansion (3.75x) was used to enhance the system signal-to-noise ratio.

The probe volume length was 2.96 mm with a diameter of 98.6 μm. The fringe spacing for the blue and green systems were 8.22 μm and 8.67 μm, respectively.

In order to obtain all three velocity components, two sets of measurements were obtained, each at a different orientation to the flow. The resulting four measured velocity components were then combined with a least squares fit in order to obtain the three components of velocity.

Polystyrene latex (PSL) spheres, manufactured using the process developed by Nichols (1987), were used as the seed material. The mean size of the seed particles varied from 0.80 μm to 0.95 μm.

Data Reduction

The station numbers given in Table 1 are the streamwise indices of the body-fitted grid at which the laser measurements were taken. The survey planes and their spanwise extent are shown in Fig. 3.

Table 1 SURVEY STATION MERIDIONAL LOCATIONS.

leading edge: J = 51; trailing edge: J = 171

Station (J)	m/m_s (%)
23	-39.7
48	-3.8
51	0.0
73	3.0
85	14.9
95	24.8
110	39.6
118*	47.5
126*	55.5
135*	64.4
156	85.2
165*	94.1
167	96.0
170	99.0

Diffuser:

Station (J)	r/r_e
172*	1.010
173	1.019
175	1.037
178	1.065

* Denotes where part flow data were taken.

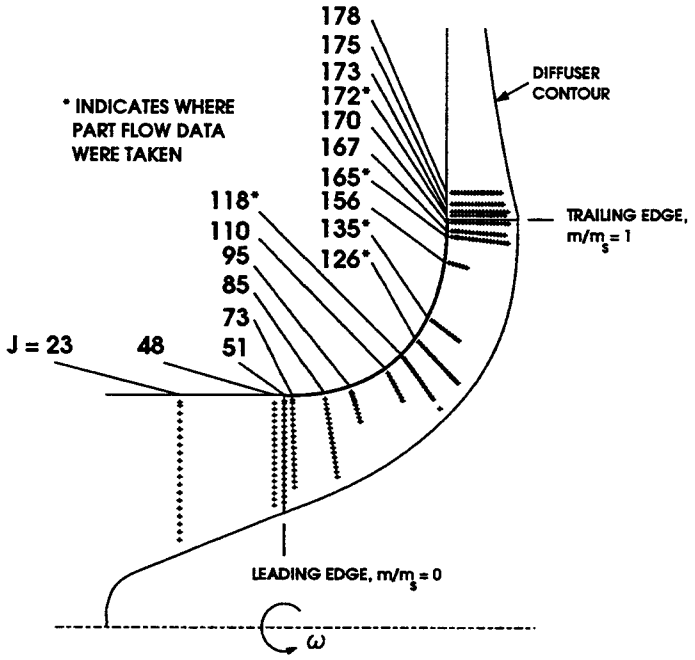

FIGURE 3. LASER ANEMOMETER SURVEY STATION LOCATIONS.

All the data are ensemble-averaged across the 20 blade channels to yield a single "representative" blade passage. This passage is divided into 1000 equal arc lengths or window "bins." For presentation purposes these bins are usually averaged down to 200 measurement locations across the blade passage. To further clarify the secondary flow vectors only every third vector is presented in the results below. This results in 66 vectors across a passage in the secondary flow results. Further details of the philosophy and the method used to obtain and average the data can be found in Strazisar et al. (1989).

Measurement Uncertainties

An estimate of the uncertainty in the calculated results was made from the least squares fit calculations. Throughout most of the impeller passage the uncertainty is estimated to be ±1.5 m/s which is about 2% of the throughflow velocity.

The measurements are susceptible to distortions of the probe volume due to window curvature effects. Due to the geometry of the laser system the spanwise velocity component is the most sensitive to measurement uncertainty. This is analogous to the difficulties in measuring the on-axis velocity component in a wind tunnel situation.

Large levels of uncertainty in the throughflow velocity exist in some isolated throughflow wake regions. Uncertainty levels approaching 15% were found to exist near some of the wake core regions.

THE CFD ANALYSIS

The computational results for the LSCC flow field were obtained using the Reynolds-averaged Navier-Stokes code developed by Dawes (1988). The code solves the equations of motion in cylindrical coordinates in integral conservation form using six-sided control volumes formed by a simple H-mesh. The basic algorithm as described by Dawes (1988) is similar to a two-step Runge-Kutta method plus residual smoothing. A combined second and fourth derivative artificial viscosity model with pressure gradient switching is used to eliminate spurious "wiggles" and to control shock capturing. The eddy viscosity is obtained using the Baldwin-Lomax (1970) mixing length model. Tip clearance is handled by gradually decreasing the thickness of the blade to zero at the blade tip and enforcing periodicity in the tip gap.

In previous calculations (Hathaway et al., 1993), it was assumed that the impeller blade tips were sharp and that in order to obtain the correct flow through the tip gap (a prime factor when considering the impact of the clearance flow on impeller aerodynamic performance) the tip clearance flow area used in the calculations would have to be reduced to account for the expected "vena contracta" produced by a sharp-edge entry. Assuming that a sharp-edged blade tip existed on the LSCC a contraction coefficient of 0.6 was used in the previous calculations. That is, the grid in the gap was modified to reduce the flow area to 60% of the physical clearance.

The blade tips of the LSCC were inspected at the end of the test program and were not found to be sharp, as expected, but instead were rounded. For a rounded tip a contraction coefficient of one would be more appropriate (Heyes et al., 1991), i.e., the flow would be expected to fill the entire physical clearance gap. The results presented here were calculated with this assumption. These calculations show much better agreement with the experimental results than previous calculations with the reduced tip gap. It is important to note, however, that the choice of using the full tip clearance in the present calculations was not based upon the experimental results but based upon the results from the blade inspection.

In addition to inspecting the blade tips of the LSCC, inspections were made of two high-speed impellers and an axial core compressor rotor for comparison. These were: a small, 6:1 pressure ratio titanium impeller; a small 4:1 pressure ratio aluminum impeller; and a 2:1 pressure ratio transonic axial flow core rotor made of maraging steel. When scaled the same the tip profiles were very similar. We conclude, therefore, that the rounding of the LSCC blade tips is not unique and should be expected in high-speed, in-service hardware. Our results show that the tip shape must be taken into account when modeling the tip clearance flow. This is true whether the tip clearance is modeled with the simplified approach of Dawes or whether the tip clearance gap is gridded with a separate blocked grid.

The grid used in the present analysis was identical to that used by Hathaway et al. (1993), with the exception that the upstream boundary was moved from 84% shroud chord upstream of the leading edge to a position on the spinner 42% of the shroud chord upstream. The boundary condition necessary for the absolute tangential velocity was obtained from a previous solution that included that particular position on the spinner as part of the computational domain. Also, the downstream extent of the grid was reduced from a radius 50% greater than the impeller exit

radius to one that was 15% greater than the exit radius. The grid had 41 points in the pitchwise direction, 71 in the spanwise direction (4 cells from blade tip to shroud), 75 points on the blade in the streamwise direction, 26 points upstream of the blade and 17 points downstream of the blade.

For the part flow calculation, the grid locations near the solid surfaces produced Y-plus values for the first cell-center ranging on the hub from 9 to 113 with an average of 53; on the shroud from 2.3 to 117 with an average of 66; on the suction surface from 35 to 211 with an average of 106; and on the pressure surface from 20 to 251 with an average of 92. The maximum for the suction surface occurred near the trailing edge at 75% span and on the pressure surface at the leading edge at 97% span. Consequently, over almost all of the computational domain the wall-function formulation of Dawes was being used to obtain wall shear stress. The amount of flow crossing the blade tips was calculated for both the design and part flow condition and was 9.4% and 11.1% of inlet mass flow, respectively.

RESULTS

The selected results below are divided into four sections: 1) throughflow development; 2) secondary flow development; 3) unusual characteristics found at station 165; and 4) the throughflow wake size and location. The part flow data were taken at five stations from the knee region to impeller exit, so that no comparison of part flow with the design condition is possible in the inducer and diffuser regions.

Throughflow Development

The throughflow velocity vector, V_T, also called quasi-meridional velocity, is defined here as the projection of the meridional velocity vector in the local meridional streamwise grid direction.

In Hathaway et al. (1993), extensive analysis of the CFD results using flow traces showed that the throughflow wake is fed primarily by the tip clearance flow. In addition, it was shown that the inducer blade boundary layers are centrifuged outward and entrained into the tip clearance flow and thereby contribute significantly to the throughflow wake.

Inducer Region at Design Flow Rate. Selected results from the inducer region at stations 85, 95 and 110 are shown in Fig. 4. The tip clearance flow is not evident in the results until station 110. The overall appearance in the inducer region is similar to that found in shrouded impellers until station 110 is reached.

The results from the CFD analysis (not shown) at the design flow condition indicate that the tip clearance flow penetration as a percent of span is 97.6%, 96.7% and 94% for stations 85, 95, and 110, respectively. This indicates why the wake does not appear in the first two stations since the measurements were taken up to 95% span for stations 85 and 95 and up to 97% span for station 110. The pitchwise location of the wake at station 110 agrees well with that predicted by the CFD analysis with the experiment showing the wake at approximately 55% pitch from the suction surface and the analysis showing it at about 62% pitch.

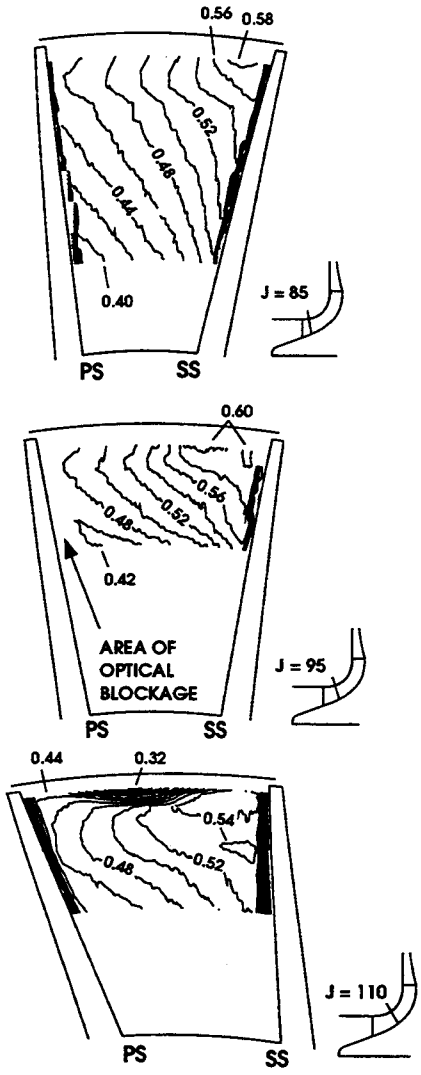

FIGURE 4. DISTRIBUTION OF EXPERIMENTAL RESULTS OF THROUGHFLOW VELOCITY COMPONENT IN THE INDUCER AT THE DESIGN FLOW NORMALIZED BY THE CORRECTED EXIT TIP SPEED (153 m/s).

Design and Part Flow CFD and Experiment. The CFD and experimental throughflow results at the design and part flow conditions are shown in Figs. 5-9. At the part flow condition, for stations 118, 126 and 135, the greater influence of the tip clearance flow on the core flow can be seen in both CFD and experiment. At station 165 the shape and level of the velocity contours are in good agreement between the experiment and CFD. At station 172 (1.01 exit radius ratio) the contours are generally in good agreement except near the suction surface where the experimental values peak near the blade wake.

This difference is probably due to the trailing edge CFD grid shape which tapers to zero whereas the actual trailing edge is blunt. At these stations the throughflow wake has migrated nearer the suction surface at the part flow condition than in the design condition as expected from secondary flow theory.

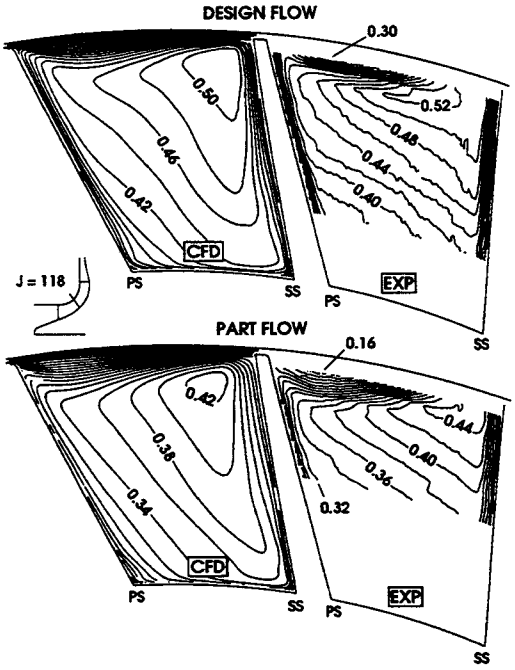

FIGURE 5. DISTRIBUTION OF THROUGHFLOW VELOCITY AT STATION 118 NORMALIZED BY THE CORRECTED EXIT TIP SPEED (153 m/s).

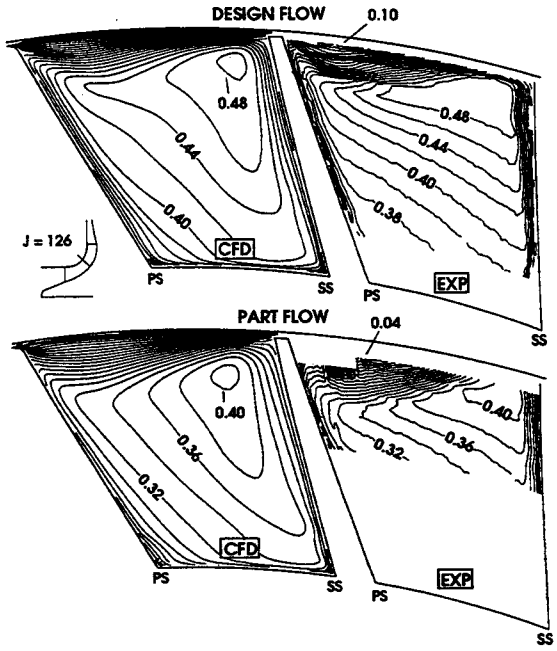

FIGURE 6. DISTRIBUTION OF THROUGHFLOW VELOCITY AT STATION 126 NORMALIZED BY THE CORRECTED EXIT TIP SPEED (153 m/s).

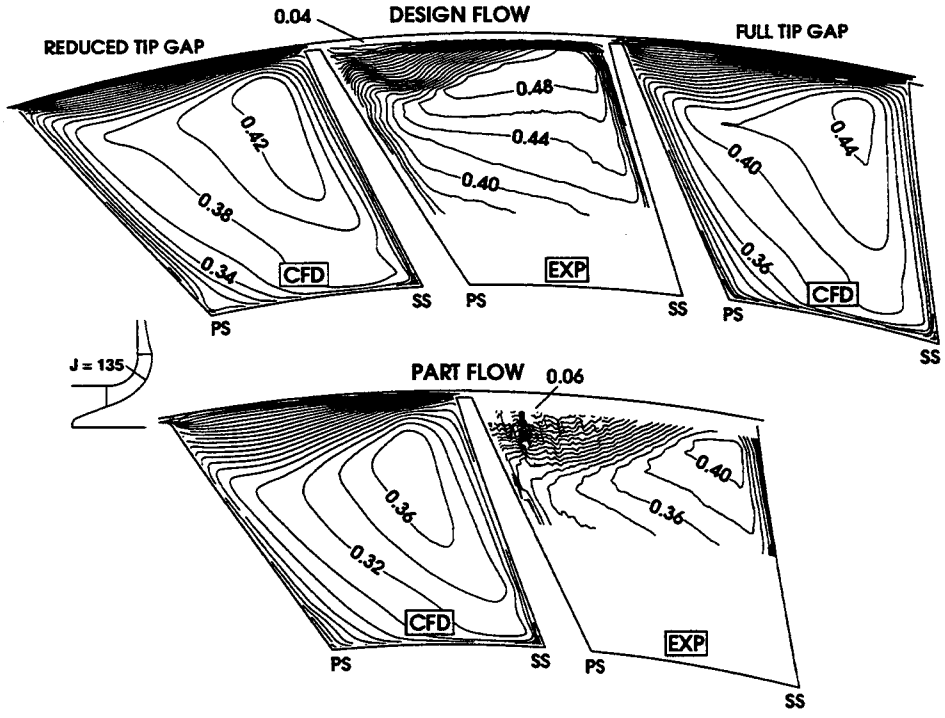

FIGURE 7. DISTRIBUTION OF THROUGHFLOW VELOCITY AT STATION 135 NORMALIZED BY THE CORRECTED EXIT TIP SPEED (153 m/s).

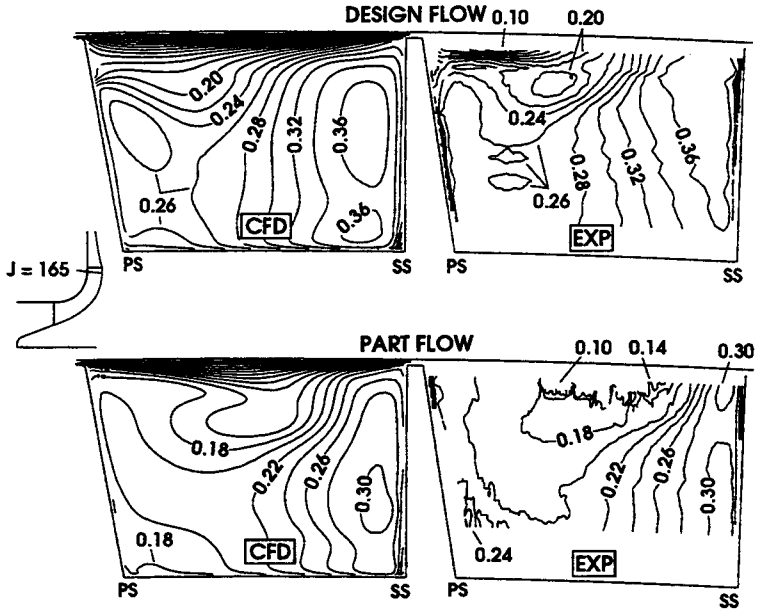

FIGURE 8. DISTRIBUTION OF THROUGHFLOW VELOCITY AT STATION 165 NORMALIZED BY THE CORRECTED EXIT TIP SPEED (153 m/s).

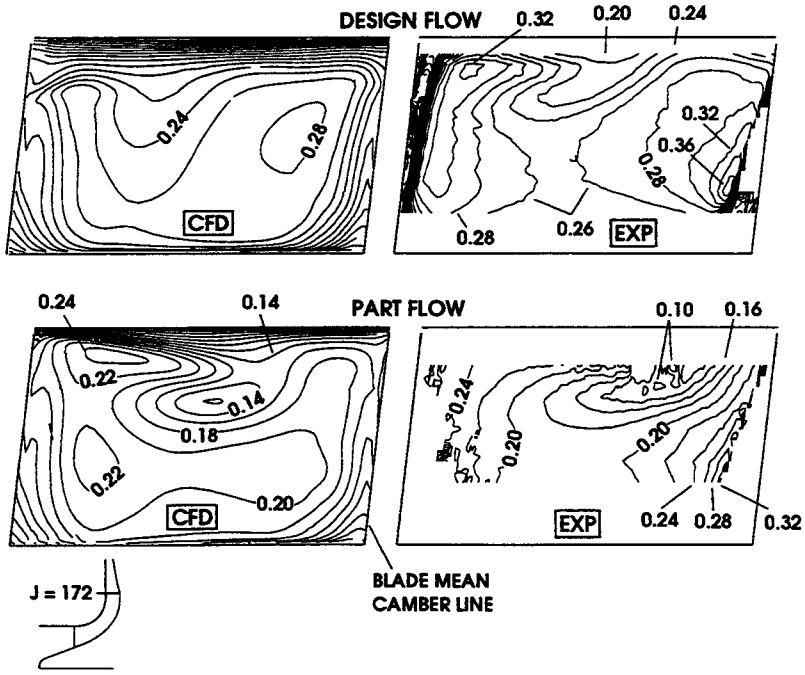

FIGURE 9. DISTRIBUTION OF THROUGHFLOW VELOCITY AT STATION 172 NORMALIZED BY THE CORRECTED EXIT TIP SPEED (153 m/s); LOOKING DOWNSTREAM.

The results from station 135, Fig. 7, show a comparison of the CFD results using two different tip gaps based on different contraction coefficients in the "vena contracta" tip clearance flow model. The CFD results on the left were obtained with a contraction coefficient of 0.6, with the initial assumption of a sharp edged blade tip (as presented in Hathaway et al., 1993). The results on the right were obtained with a contraction coefficient of 1.0 which is representative of the actual tip shape. These results show the sensitivity of wake size to a change in flow rate through the tip clearance gap.

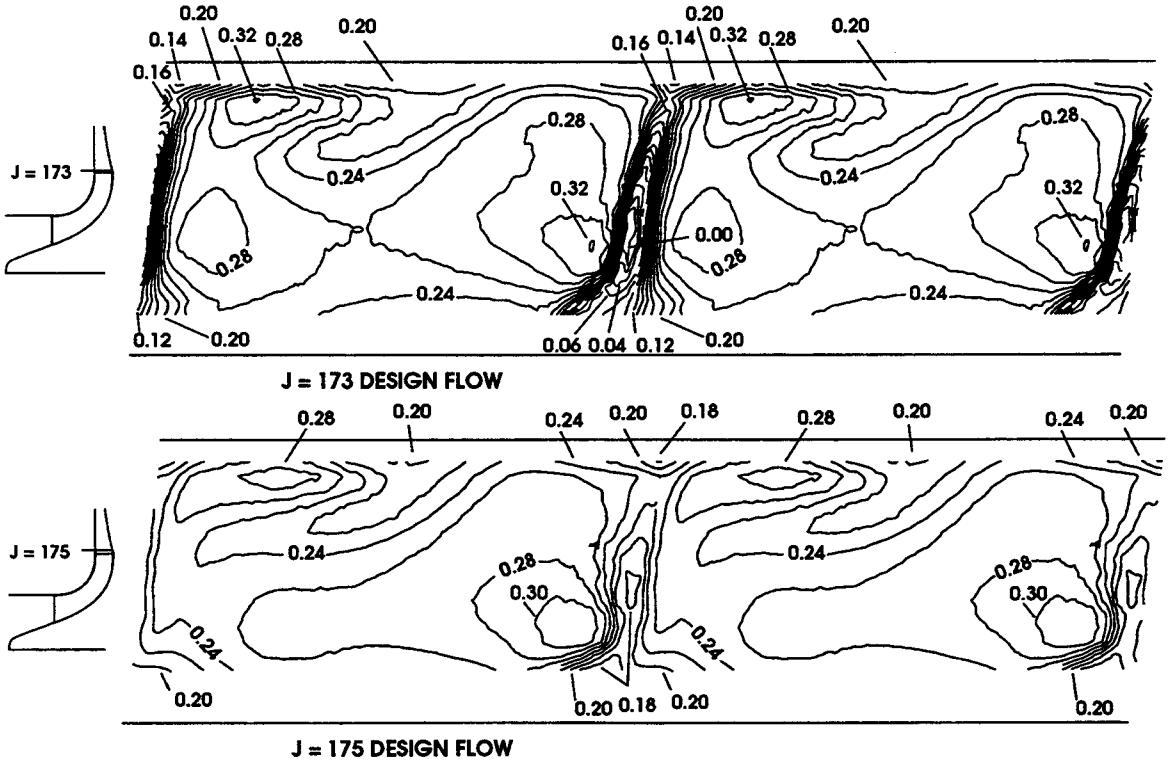

FIGURE 10. DISTRIBUTION OF EXPERIMENTAL RESULTS OF THROUGHFLOW VELOCITY WITH DUPLICATE PASSAGES AT STATIONS 173 AND 175, NORMALIZED BY THE CORRECTED EXIT TIP SPEED (153 m/s); LOOKING DOWNSTREAM.

Diffuser at Design. Experimental throughflow results for stations 173 and 175 at the design condition are shown in Fig. 10. A high degree of mixing takes place in the blade wake region between these two stations. This was shown in Hathaway et al. (1993), in terms of the change in absolute flow angle. The high shear in the blade wake produces intense mixing from the trailing edge to station 175 at which location the gradients in the blade wake and throughflow wake become similar and mixing is greatly reduced. From station 175 (r/r_e = 1.037) to station 178, not shown, (r/r_e = 1.065) there is little additional mixing of the flow which would indicate that placing diffuser vanes at a radius ratio greater than about 4% of the impeller exit radius would do little to provide a more uniform flow into the diffuser. Other conditions such as pressure perturbations from diffuser vanes upon the impeller exit flow, which may produce deeper blade wakes, could moderate this conclusion.

Comparison of Secondary Flow Development

Secondary flow in this paper is defined as the departure of the local relative velocity vector from the local streamwise grid direction. The secondary flow vector is given by $\mathbf{W}_{sec} = \hat{\mathbf{g}} \times (\mathbf{W} \times \hat{\mathbf{g}})$. The spanwise and pitchwise components of the secondary velocity vector are the projections of the secondary velocity vector in the local spanwise and pitchwise grid directions.

The secondary flow vector results are especially sensitive to uncertainties in the measured velocities. Areas that show chaotic appearance of the secondary vectors, therefore, are suspect in that they are areas where flow unsteadiness or passage-to-passage variations are possible. It has been our experience that in wake type regions measurement uncertainty cannot be decreased significantly by increasing the number of measurements. The results presented herein have been ensemble averaged, and thus the contributions of flow unsteadiness and passage-to-passage variations to measurement uncertainty cannot be separated out. However, we have inspected the measurements in numerous locations and found that the contribution from passage-to-passage variations is generally very small. Therefore, we generally attribute large values of uncertainty in wake regions to flow unsteadiness.

Similar secondary flow development for both flow rates is evident at stations 118 through 135 (Fig. 11). CFD particle traces (not shown here) confirm that the tip clearance flow penetrates across the channel and impinges on the pressure surface for both flow conditions. However, greater spanwise penetration is exhibited at the part flow condition.

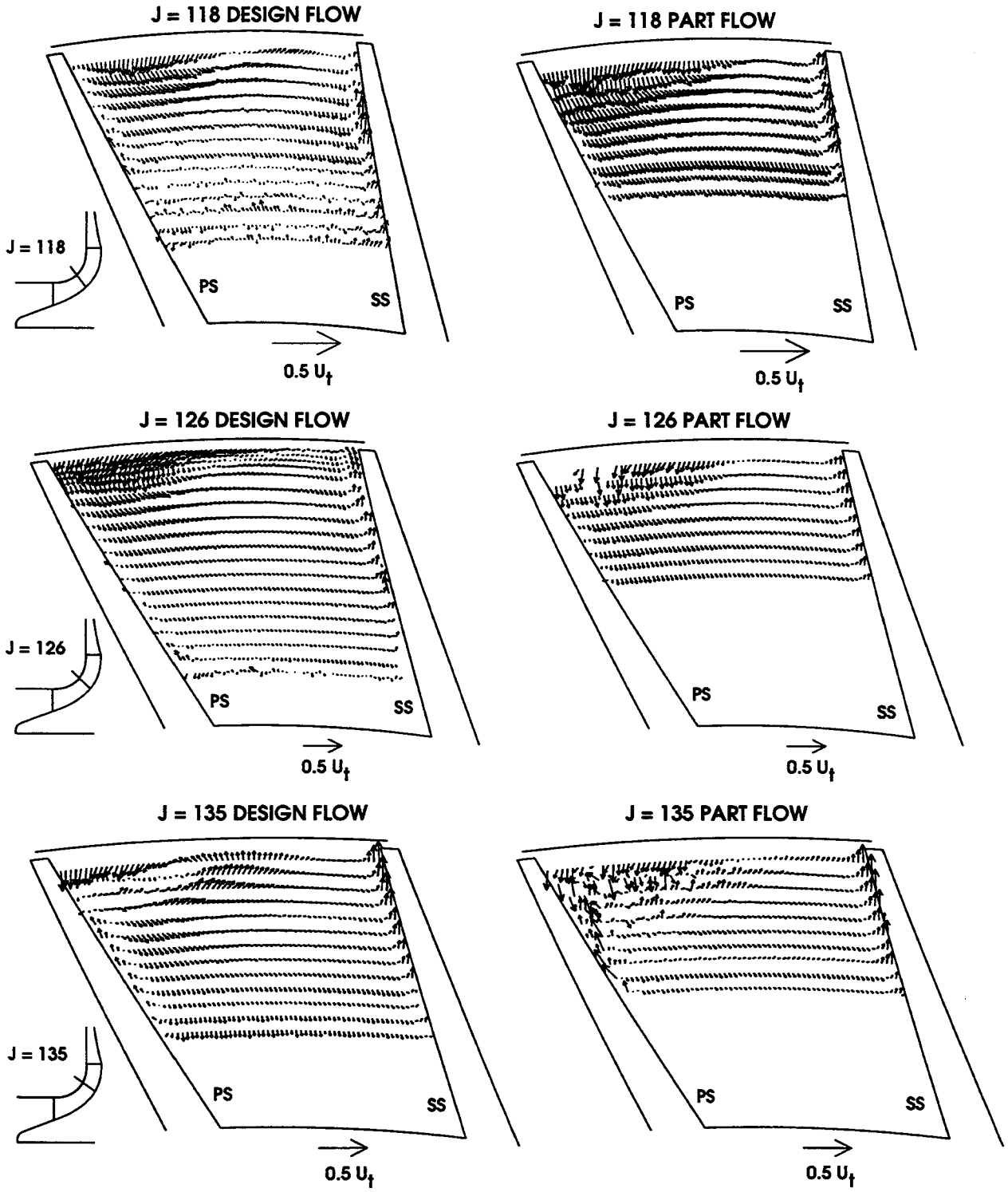

FIGURE 11. MEASURED SECONDARY FLOW VECTORS IN THE KNEE REGION AT DESIGN AND PART FLOW CONDITIONS.

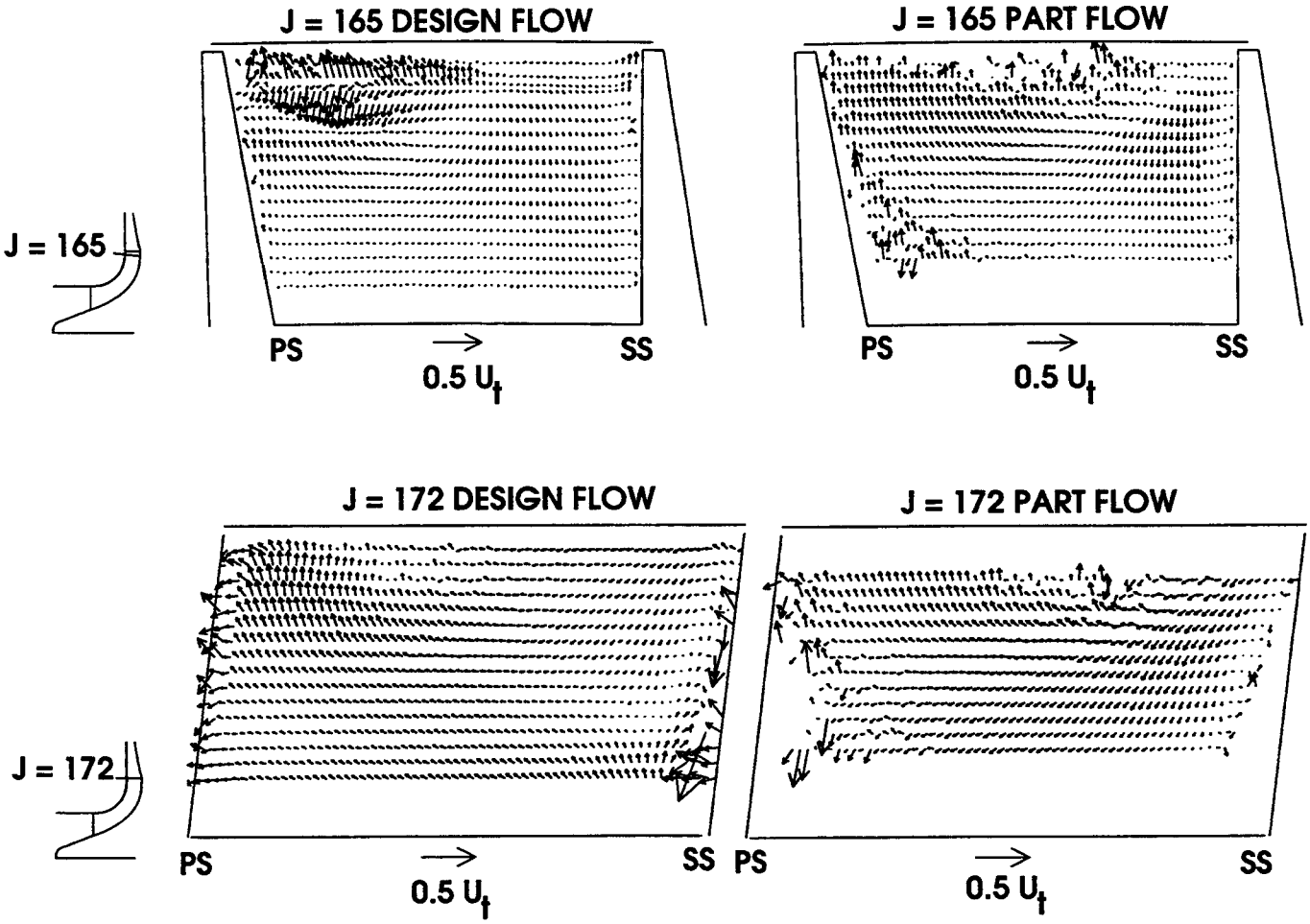

FIGURE 12. MEASURED SECONDARY FLOW VECTORS NEAR THE IMPELLER EXIT AT DESIGN AND PART FLOW CONDITIONS; LOOKING DOWNSTREAM.

It is evident from these figures that the throughflow wake development occurs earlier in the impeller at the part flow condition relative to the design condition, e.g., the flow at station 118 at part flow appears similar to that of 126 at design flow. This is noted also in the CFD results, which are not shown here.

The unusual flow pattern at station 165 (Fig. 12) begins development at station 156 (not shown) and is dissipating by station 167 (also not shown). The origins of this flow structure are at present unknown. Some evidence for flow unsteadiness is noted in the part flow case near the hub pressure surface corner at station 165. This is discussed further in the following section.

Station 165 Wake Fluctuations

Considerable effort has been expended in order to investigate the secondary flow vector results at station 165 for both the design and part flow conditions. At the design condition the unusual bifurcation pattern near the throughflow wake sparked interest as did the results at part flow near the pressure side/hub corner. These investigations are described in the following.

Design. In Hathaway et al. (1993), it was shown in the design flow case that the flow pattern at 165 would look similar to the pattern at 172 if the mode of the measurements was used in the determination of each velocity component as opposed to the mean, which is normally used. The mode is by definition what the flow is doing "most of the time," i.e., it is the most probable value. This leads one to believe that some unsteadiness of unknown origin may be present at station 165.

In an attempt to determine the origin of this possible unsteadiness a set of measurements were acquired such that the tangential and throughflow components were measured directly while in the "coincident" data acquisition mode. The coincident mode insures that velocity measurements from each of the two laser anemometer channels arise from the same particle. This raises the statistical confidence in the $V_T' V_\theta'$ correlation which will be described further below.

These results were ensemble averaged onto a representative "revolution," or all twenty passages, rather than a single passage (as is done for the other results in this paper). If there were

geometric variations contributing to the uncertainty, they would be detected as a passage-to-passage variation in this average.

No significant variation from passage-to-passage could be detected. In addition, the $V_T' V_\theta'$ correlation showed that the fluctuations could not be attributed to any organized flow pumping in either the throughflow or tangential directions. That is, if V_T' and V_θ' were positively correlated it would indicate fluctuations primarily in magnitude with minimal fluctuations in absolute flow angle. If they were negatively correlated it would indicate (because of the local velocity triangle) that flow angle fluctuations were greater than fluctuations in magnitude.

Without any indication of an organized fluctuation in the throughflow–tangential plane, we therefore conclude that the variation in the secondary vectors in the throughflow wake region is primarily associated with fluctuations in the spanwise component of velocity. This could be precipitated by wandering or kinking of the clearance vortex as noted in axial flow pump research by Straka and Farrell (1992), and Zierke et al. (1993).

Part Flow. In the secondary flow results at station 165, some indication of flow unsteadiness is noted in the chaotic behavior of the vectors near the hub, pressure surface corner and in the wake. The secondary flow vector results are very sensitive to fluctuations in any of the velocity component measurements. An investigation similar to that described above was undertaken in order to look for stalled passages (i.e., passage-to-passage variation).

No stalled passages were found in the analysis. Moreover, line plots of the throughflow velocity (shown in Fig. 13), along with uncertainty limits (based on a 95% confidence level), show no indication of a flow separation, although the fluctuation levels in this region were very high (30% of the mean flow levels). Note that the regions of high uncertainty correspond to regions of chaotic behavior in the secondary flow vectors of Fig. 12.

Wake Size and Location

Hathaway et al. (1987), and Suder et al. (1987) observed that the strength of the velocity fluctuations which are uncorrelated with the fundamental rotor rotational frequency (e.g., velocity fluctuations due to turbulence, vortex shedding, etc.) can be used as an effective marker to locate the wakes within turbomachinery. The strength of these uncorrelated velocity fluctuations (denoted by Hathaway as "unresolved unsteadiness") is measured by the local (relative to the rotor) standard deviation of the laser velocimeter measurements. The wake regions shown in Fig. 14a were determined from contour plots of the standard deviation of one of the laser velocimeter channels. The wake boundary is arbitrarily defined here as 50% of the peak standard deviation outside of the blade boundary layers in each of the cross-channel planes. The wake location given in Fig. 14b is the approximate wake center determined by inspection of Fig. 14a.

Relative to the design flow results, the part flow results show a slight increase in wake size up to station 135 and a decrease in wake size near the impeller exit. The CFD results support the observed wake size behavior in the experiment between the two flow rates. A comparison of the CFD distribution of the clearance flow for both flow conditions is given in Fig. 15a. The cumulative

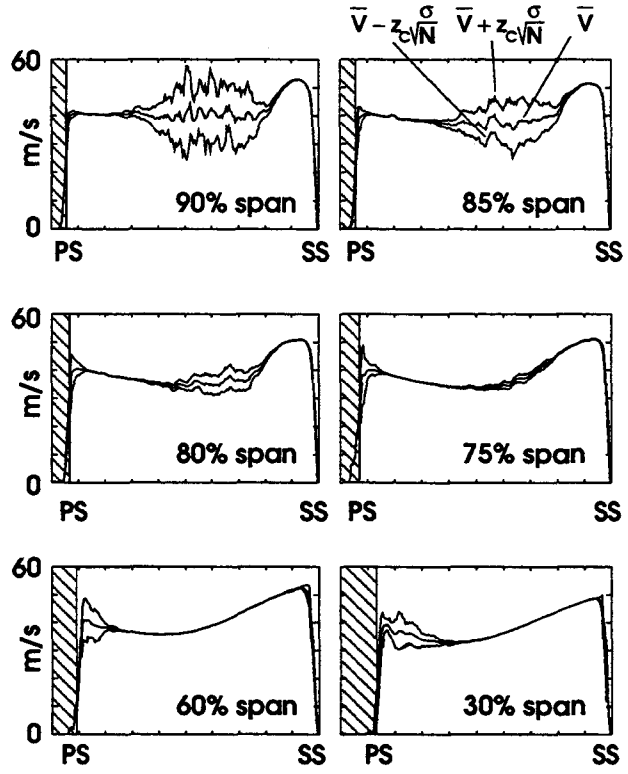

FIGURE 13. PLOTS OF THROUGHFLOW MEAN VELOCITY COMPONENT WITH LOCAL UNCERTAINTY LIMITS AT STATION 165 AT PART FLOW. THE UNCERTAINTY IS GIVEN BY $z_c \frac{\sigma}{\sqrt{N}}$ WHERE z_c = 1.96 FOR A 95% CONFIDENCE LEVEL.

clearance flow is plotted versus meridional distance and shows that the clearance flow for the part flow case exceeds that for the design flow case until about 65% chord which corresponds to station 135 in the laser measurements. After 65% chord the clearance flow for the part flow case becomes less than for the design flow case until it is lower by 17% at impeller exit. This corresponds well to the qualitative distribution of the wake size shown in Fig. 14a. A detailed look at the clearance flow per unit chord along the meridional direction is shown in Fig. 15b. The clearance flow per unit chord for the part flow case exceeded that for the design flow up to 8% chord after which it was less than for the design flow case.

A comparison of the CFD predicted and experimentally measured blade pressure loadings revealed that the leading edge region for the part flow case is more heavily loaded than for the design flow case due to increased incidence but that the rest of the blade pressure loading is less than for the design flow case. Consequently, we can conclude that the wake size increase in the inducer region is due to increased incidence at part flow and that the apparent smaller wake size in the exit region is a result of decreased pressure difference across most of the blade which results in a decrease in clearance flow per unit chord over the aft 92% of the blade.

A reduction in blade pressure loading with increased overall pressure rise for the part flow case is not intuitively obvious, but

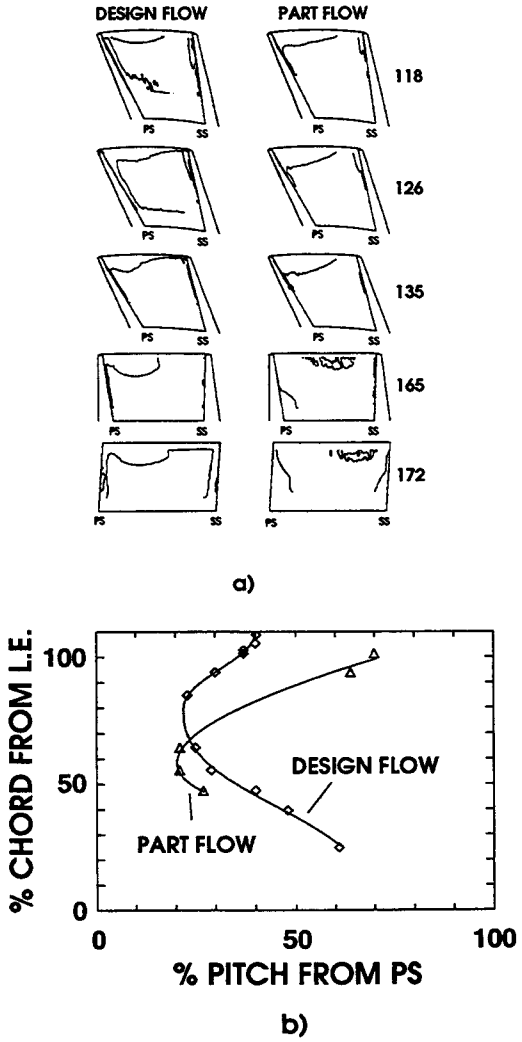

FIGURE 14. A) WAKE BOUNDARY CONTOURS SHOWN ARE AT 50% OF THE PEAK VALUE OUTSIDE OF THE BLADE BOUNDARY LAYERS. B) APPROXIMATE THROUGHFLOW WAKE LOCATION AS A FUNCTION OF CHORD FOR BOTH THE DESIGN AND PART FLOW CONDITIONS.

it can be easily shown from the tangential momentum equation for near radial flow in an impeller that the pressure difference across the channel is given by

$$\Delta p = \frac{2\pi}{N_B}(2V_r V_\theta)\rho.$$

In the radial portion of the impeller, the radial velocity varies with the mass flow rate and, thus, it is clear that the reduction in blade pressure loading with reduced flow rate is a logical consequence. Noting this and the results of the measured wake location from Fig. 14 b, it is clear that an increase in cross-channel pressure loading cannot be responsible for the movement of the wake closer to the suction surface for the part flow condition as one might intuitively expect.

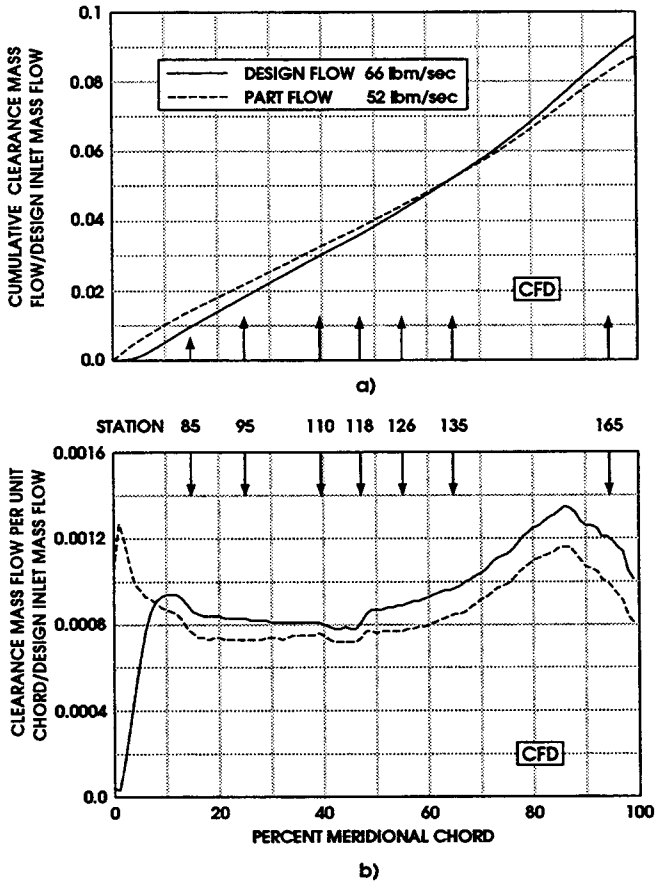

FIGURE 15. CFD RESULTS OF TIP CLEARANCE MASS FLOW. A) CUMULATIVE MASS FLOW. B) CLEARANCE MASS FLOW PER UNIT CHORD.

Morris and Kenny (1971) proposed using $\Delta p/2q$, as a measure of blade loading and hence propensity for secondary flow development. This is the ratio of the cross-channel pressure gradient to the dynamic head and is similar to the rotation number (ratio of Coriolis acceleration to inertial acceleration). The expression can be simplified for a radial impeller to

$$\frac{\Delta p}{2q} = \frac{4\pi r\omega}{N_B V_r}.$$

For a radial bladed impeller this is a measure of the imbalance in forces that occur on a low velocity fluid when subjected to a transverse pressure gradient set up by a higher velocity mainstream. We conclude that the freestream dynamic head decreases faster than the blade pressure loading as the flow rate decreases so that the net result is for the low velocity wake fluid to exit the impeller closer to the suction surface.

To insure that the measured and CFD blade pressure loadings versus mass flow rate characteristic is not unique to this impeller, we compared the variation in blade pressure loading based upon overall experimentally measured quantities for the present impeller to that of two high pressure ratio impellers. These impellers had pressure ratios of 6:1 and 4:1. From overall power

input the blade pressure loading can be related to overall performance through

$$\Delta p \propto \dot{m}\frac{\Delta H}{\omega}.$$

The same trend of reduced blade loading with decreasing flow rate was found in both high pressure ratio impellers for flow rates below about 96%–98% of choking flow. Near choke the total enthalpy rise decreases at constant mass flow rate so that the trend does not hold.

CONCLUSIONS

Detailed measurements and 3D viscous calculations of the LSCC velocity field at two different flow rates have demonstrated the ability of modern computational tools to reasonably simulate the flow in a centrifugal compressor which contains no large streamwise separation. The tip clearance flow which constitutes a large portion of the throughflow wake impinges upon the pressure surface sooner and then moves further toward the suction surface as the flow rate is reduced. It was shown that the movement of the throughflow wake closer to the suction surface as the flow was reduced from design flow to part flow was not a result of an increased pressure difference across the blade channel. Both CFD and experiment showed that the cross channel pressure difference decreased as flow was reduced. The movement of the throughflow wake toward the suction surface is consistent with well-known non-dimensional factors used to characterize the migration of low velocity fluid subjected to transverse pressure gradients imposed by a higher velocity freestream fluid. These features are accurately captured by the computations. The throughflow wake at the impeller exit was slightly smaller at the lower flow rate which was consistent with the clearance flows obtained from the CFD analysis.

The importance of accurately knowing not only the tip clearance gap but the physical shape of the blade tip (whether due to in-service wear or initial manufacture) was demonstrated and emphasizes further the importance of adequately knowing the "as-tested" geometry when predicting impeller aerodynamic performance.

The computational results presented confirm the ability of modern computational tools to accurately model the dynamics of a subsonic centrifugal compressor impeller when such pertinent geometrical parameters as tip clearance and blade tip shape are accurately known. The ability to predict development of the throughflow wake which is largely fed by the tip clearance flow as the impeller is throttled should give designers much better confidence in using computational tools to improve impeller performance.

REFERENCES

Adler, D., and Levy, Y., 1979, "A Laser-Doppler Investigation of the Flow Inside a Backswept, Closed, Centrifugal Compressor", *Journal of Mechanical Engineering Science*, Vol. 21, No. 1.

Ahmed, N. A., and Elder, R. L., 1990, "Flow Investigation in a Small High Speed Impeller Passage Using Laser Anemometry", ASME Paper No. 90-GT-233.

Baldwin, B., and Lomax, H., 1970, "Thin Layer Approximation and Algebraic Model for Separated Turbulent Flows", AIAA Paper No. 78–257.

Cumpsty, N. A., 1989, *Compressor Aerodynamics*. Longman Scientific and Technical.

Dawes, W. N., 1988, "Development of a 3-D Navier Stokes Solver of Application to all Types of Turbomachinery", ASME Paper 88-GT-70.

Dean, R., and Senoo, Y., 1960, "Rotating Wakes in Vaneless Diffusers", *ASME Journal of Basic Engineering*, Vol. 82, No. 3, 563–574, Sept.

Eckardt, D., 1976, "Detailed Flow Investigations Within a High-Speed Centrifugal Compressor Impeller", *ASME Journal of Fluids Engineering*, Vol. 98, No. 3, 390–402, Sept.

Fagan, J. R., and Fleeter, S., 1990, "Impeller Flow Field Measurement and Analysis", *ASME Journal of Turbomachinery*, Vol. 113, No. 4, 670–679.

Farge, T. Z., and Johnson, M. W., 1990, "The Effect of Backswept Blading on the Flow in a Centrifugal Compressor Impeller", ASME Paper 90–GT-231.

Hathaway, M. D., Chriss, R. M., Wood, J. R., and Strazisar, A. J., 1993, "Experimental and Computational Investigation of the NASA Low-Speed Centrifugal Compressor Flow Field", *ASME Journal of Turbomachinery*, Vol. 115, No. 3, 527–542.

Hathaway, M. D., Suder, K. L., Okiishi, T. H., Strazisar, A. J., and Adamczyk, J. J., 1987, "Measurements of the Unsteady Flow Field Within the Stator Row of a Transonic Axial-Flow Fan, Part II - Results and Discussion", ASME Paper No. 87–GT-227.

Hathaway, M. D., Wood, J. R., and Wasserbauer, C. W., 1992, "NASA Low Speed Centrifugal Compressor for 3-D Viscous Code Assessment and Fundamental Flow Physics Research", *ASME Journal of Turbomachinery*, Vol. 114, No. 2, 295–303.

Heyes, F. J. G., Hodson, H. P., and Dailey, G. M., 1991, "The Effect of Blade Tip Geometry on the Tip Leakage Flow in Axial Turbine Cascades", ASME Paper No. 91–GT-135.

Johnson, M. W., and Moore, J., 1983, "The Influence of Flow Rate on the Wake in a Centrifugal Impeller", *ASME Journal of Engineering for Power*, Vol. 105, No. 1, 33–39.

Krain, H., 1981, "A Study on Centrifugal Impeller and Diffuser Flow", *Journal of Engineering for Power*, Vol. 103, No. 4, 688–697.

Krain, H., 1988, "Swirling Impeller Flow", *ASME Journal of Turbomachinery*, Vol. 110, No. 1.

Krain, H., and Hoffmann, W., 1989, "Verification of an Impeller Design by Laser Measurements and 3D-Viscous Flow Calculations", ASME Paper No. 89-GT-159.

Krain, H., and Hoffmann, W., 1990, "Centrifugal Impeller Geometry and its Influence on Secondary Flows", In *Secondary Flows in Turbomachines* (1990), AGARD.

Morris, R. E., and Kenny, D. P., 1971, "High Pressure Ratio centrifugal Compressors for Small Gas Turbine Engines", In *Advanced Centrifugal Compressors* (1971), R. C. Dean, Ed., ASME.

Nichols, C. E., 1987, "Preparation of Polystyrene Microspheres for Laser Velocimetry in Wind Tunnels", NASA TM 89163.

Rohne, K. H., and Banzhaf, M., 1990, "Investigation of the Flow at the Exit of an Unshrouded Centrifugal Impeller and Comparison With the Classical Jet-Wake Theory", *ASME Journal of Turbomachinery*, Vol. 113, No. 4, 654–659.

Sipos, G., 1991, "Secondary Flow Loss Distribution in a Radial Compressor with Untwisted Backswept Vanes", *ASME Journal of Turbomachinery*, Vol. 113, No. 4, 686–695.

Straka, W. A., and Farrell, K. J., 1992, "The Effect of Spacial Wandering on Experimental Laser Velocimeter Measurements of the End-Wall Vortices in an Axial Flow Pump", *Experiments in Fluids*, Vol. 13, No. 2, 163–170.

Strazisar, A. J., Wood, J. R., Hathaway, M. D., and Suder, K. L., 1989, "Laser Anemometer Measurements in a Transonic Axial-Flow Fan Rotor", NASA TP-2879.

Suder, K. L., Hathaway, M. D., Okiishi, T. H., Strazisar, A. J., and Adamczyk, J. J., 1987, "Measurements of the Unsteady Flow Field Within the Stator Row of a Transonic Axial-Flow Fan, Part I - Measurement and Analysis Technique", ASME Paper No. 87–GT–226.

Wood, J. R., Adam, P. W., and Buggele, A. E., 1983, "NASA Low-Speed Centrifugal Compressor for Fundamental Research", NASA TM 83398.

Wood, J. R., Strazisar, A. J., and Hathaway, M. D., 1990, "E/C0-2 Single Transonic Fan Rotor", In *AGARD AR-275* (1990).

Zierke, W. C., Straka, W. A., and Taylor, P. D., 1993, "The High Reynolds Number Flow Through an Axial-Flow Pump", The Pennsylvania State University, Applied Research Laboratory, TR-93–12.